Pure Spin Current Injection in Hydrogenated Graphene Structures

Reinaldo Zapata-Peña, Bernardo S. Mendoza, Anatoli I. Shkrebtii

1 Introuction

sec:introuction

Filling with text.

Lorem ipsum dolor sit amet, consectetuer adipiscing elit. Etiam lobortis facilisis sem. Nullam nec mi et neque pharetra sollicitudin. Praesent imperdiet mi nec ante. Donec ullamcorper, felis non sodales commodo, lectus velit ultrices augue, a dignissim nibh lectus placerat pede. Vivamus nunc nunc, molestie ut, ultricies vel, semper in, velit. Ut porttitor. Praesent in sapien. Lorem ipsum dolor sit amet, consectetuer adipiscing elit. Duis fringilla tristique neque. Sed interdum libero ut metus. Pellentesque placerat. Nam rutrum augue a leo. Morbi sed elit sit amet ante lobortis sollicitudin. Praesent blandit blandit mauris. Praesent lectus tellus, aliquet aliquam, luctus a, egestas a, turpis. Mauris lacinia lorem sit amet ipsum. Nunc quis urna dictum turpis accumsan semper.

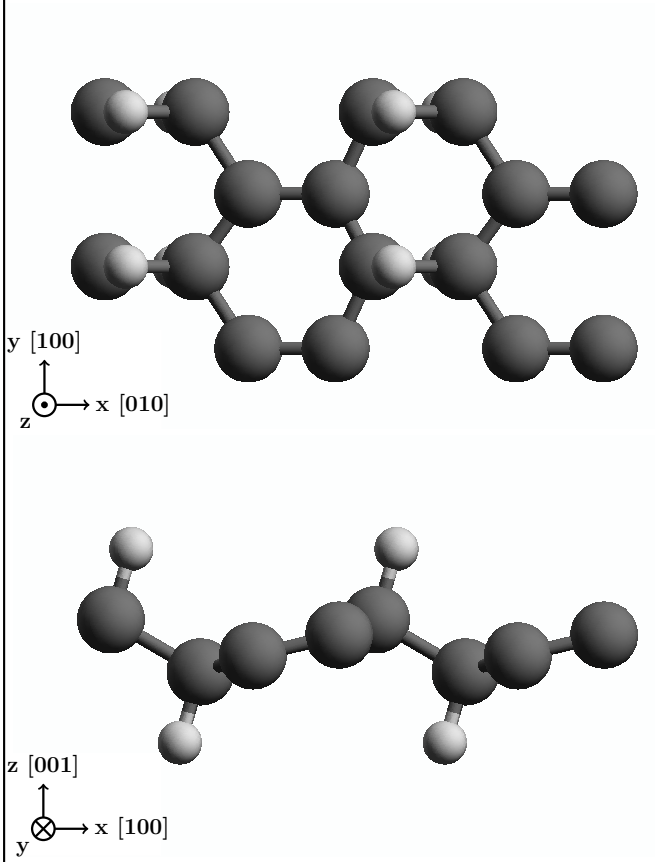

Figure 1: Alt structure. fig:altstruc

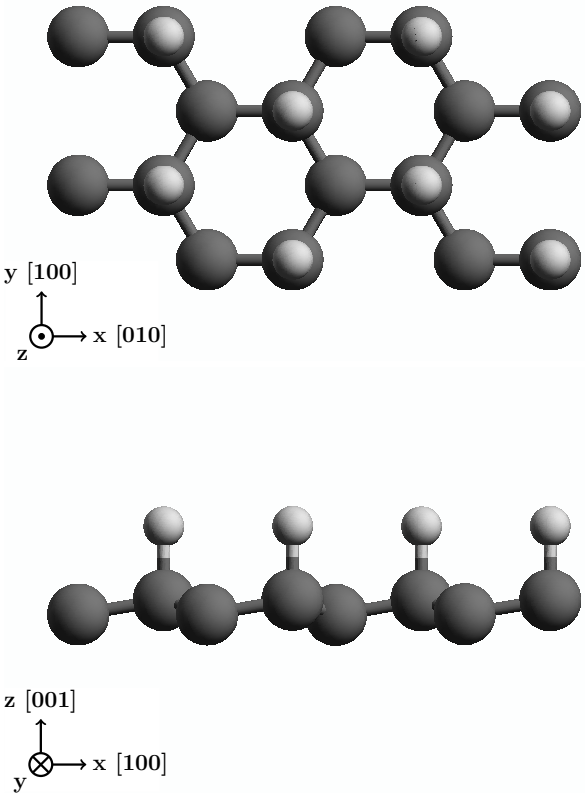

Figure 2: Up structure fig:upstruc

Lorem ipsum dolor sit amet, consectetuer adipiscing elit. Etiam lobortis facilisis sem. Nullam nec mi et neque pharetra sollicitudin. Praesent imperdiet mi nec ante. Donec ullamcorper, felis non sodales commodo, lectus velit ultrices augue, a dignissim nibh lectus placerat pede. Vivamus nunc nunc, molestie ut, ultricies vel, semper in, velit. Ut porttitor. Praesent in sapien. Lorem ipsum dolor sit amet, consectetuer adipiscing elit. Duis fringilla tristique neque. Sed interdum libero ut metus. Pellentesque placerat. Nam rutrum augue a leo. Morbi sed elit sit amet ante lobortis sollicitudin. Praesent blandit blandit mauris. Praesent lectus tellus, aliquet aliquam, luctus a, egestas a, turpis. Mauris lacinia lorem sit amet ipsum. Nunc quis urna dictum turpis accumsan semper. Lorem ipsum dolor sit amet, consectetuer adipiscing elit. Etiam lobortis facilisis sem. Nullam nec mi et neque pharetra sollicitudin. Praesent imperdiet mi nec ante. Donec ullamcorper, felis non sodales commodo, lectus

velit ultrices augue, a dignissim nibh lectus placerat pede. Vivamus nunc nunc, molestie ut, ultricies vel, semper in, velit. Ut porttitor. Praesent in sapien. Lorem ipsum dolor sit amet, consectetuer adipiscing elit. Duis fringilla tristique neque. Sed interdum libero ut metus. Pellentesque placerat. Nam rutrum augue a leo. Morbi sed elit sit amet ante lobortis sollicitudin. Praesent blandit blandit mauris. Praesent lectus tellus, aliquet aliquam, luctus a, egestas a, turpis. Mauris lacinia lorem sit amet ipsum. Nunc quis urna dictum turpis accumsan semper. Lorem ipsum dolor sit amet, consectetuer adipiscing elit. Etiam lobortis facilisis sem. Nullam nec mi et neque pharetra sollicitudin. Praesent imperdiet mi nec ante. Donec ullamcorper, felis non sodales commodo, lectus velit ultrices augue, a dignissim nibh lectus placerat pede. Vivamus nunc nunc, molestie ut, ultricies vel, semper in, velit. Ut porttitor. Praesent in sapien. Lorem ipsum dolor sit amet, consectetuer adipiscing elit. Duis fringilla tristique neque. Sed interdum libero ut metus. Pellentesque placerat. Nam rutrum augue a leo. Morbi sed elit sit amet ante lobortis sollicitudin. Praesent blandit blandit mauris. Praesent lectus tellus, aliquet aliquam, luctus a, egestas a, turpis. Mauris lacinia lorem sit amet ipsum. Nunc quis urna dictum turpis accumsan semper.

2 Theory

sec:theory

The equation for $\mathcal{V}^{ab}$ for normal incidence in the xy plane with a polarization angle α is given by

$$\begin{aligned}\mathcal{V}^{ab}(\omega) &= \frac{\mu^{abxx}(\omega)E^2(\omega)\cos^2(\alpha)+\mu^{abyy}(\omega)E^2(\omega)\sin^2(\alpha)+2\mu^{abxy}(\omega)E^2(\omega)\cos(\alpha)\sin(\alpha)}{\xi^{xx}(\omega)E^2(\omega)\cos^2(\alpha)+\xi^{yy}(\omega)E^2(\omega)\sin^2(\alpha)},\\ &= \frac{\mu^{abxx}(\omega)\cos^2(\alpha)+\mu^{abyy}(\omega)\sin^2(\alpha)+2\mu^{abxy}(\omega)\cos(\alpha)\sin(\alpha)}{\xi^{xx}(\omega)\cos^2(\alpha)+\xi^{yy}(\omega)\sin^2(\alpha)}. \qquad (1)\end{aligned}$$

eq:vab

For an angle $\alpha=\frac{\pi}{4}$ this expression can be reduced to

$$\mathcal{V}^{ab}(\omega)=\frac{\mu^{abxx}(\omega)+\mu^{abyy}(\omega)+2\mu^{abxy}(\omega)}{\xi^{xx}(\omega)+\xi^{yy}(\omega)}. \qquad (2)$$

eq:vab-90deg

We also define $|\mathcal{V}^a|$ as

$$|\mathcal{V}^a|=\sqrt{(\mathcal{V}^{ax})^2+(\mathcal{V}^{ay})^2+(\mathcal{V}^{az})^2}, \qquad (3)$$

eq:vab-mag

and the corresponding polar and azimuthal angles θ and φ as

$$\theta=\cos^{-1}\left(\frac{\mathcal{V}^{az}}{|\mathcal{V}^a|}\right), \qquad 0\leq\theta\leq\pi, \qquad (4)$$

eq:polar-ang

$$\varphi=\tan^{-1}\left(\frac{\mathcal{V}^{ay}}{\mathcal{V}^{ax}}\right), \qquad 0\leq\varphi\leq 2\pi. \qquad (5)$$

eq:azimuthal-ang

(6)

3 Results

sec:results

We preset the results for $\mathcal{V}^{ab}$ for the $C_{16}H_8$-alt and $C_{16}H_8$-up structures being both noncentrosymmetric semi-infinite carbon systems with 50% hydrogenation in different arrangements. The *alt* system has alternating hydrogen atoms on the upper and bottom sides of the carbon sheet, while the *up* system has H only on the upper side. We take the hexagonal carbon lattice to be on the xy plane for both structures, and the carbon-hydrogen bonds on the perpendicular xz plane, as depicted in Figs. 1 and 2.

Using the ABINIT code [1] we calculated the self- consistent ground state and the Kohn-Sham states using density functional theory in the local density approximation (DFT-LDA) with a planewave basis. We used Hartwigsen- Goedecker-Hutter (HGH) relativistic separable dual-space Gaussian pseudopotentials [2] including the spin-orbit interaction for calculating $\mathcal{V}^a(\omega)$.

The convergence parameters for the calculations of our results corresponding to the *alt* and *up* structures are cutoff energies of 65 Ha and 40 Ha, respectively. The energy eigenvalues and matrix elements were calculated using 14452 **k** points and 8452 **k** points in the irreducible Brillouin zone (IBZ) and present LDA energy band gaps of 0.72 eV and 0.088 eV, respectively for the *alt* and *up* structures. As mentioned in [4], using DFT the LDA is only one method of many other that can be used to calculate the electronic structure of materials. Also it is known that all methods predict a different band gap than the obtained in the experiment. A correction for the band gap energy value can be calculated by other *ab-initio* methods such as the GW approximation [3] being this outside the scope of this paper.

The structures presented here where divided into layers to analyze the he layer- by-layer contribution for $\mathcal{V}^{ab}$ response. The *alt* structure was divided in six layers corresponding the first one to the top hydrogen atoms, from the second to the forth to carbon atoms in different z positions, and the sixth and last one to the bottom hydrogen atoms. The *up* structure was divided into two layers, the first one comprised by the top hydrogen atoms and the second by the carbon atoms. The layer divisions and atom positions for the unit cells are shown in Tables 1 and 2.

Layer No.	Atom type	Position [Å]		
		x	y	z
1	H	-0.61516	-1.42140	1.47237
2	C	-0.61516	-1.73300	0.39631
3	C	0.61516	1.73300	0.15807
4	C	0.61516	0.42201	-0.15814
5	C	-0.61516	-0.37396	-0.39632
6	H	-0.61516	-0.68566	-1.47237

Table 1: Unit cell of *alt* structure. Layer division, atom types and positions for the *alt* structure. The structure unit cell was divided in six layers corresponding each one to atoms in different z positions. tab:altunitcell

Layer No.	Atom type	Position [Å]		
		x	y	z
1	H	-0.61516	-1.77416	0.73196
1	H	0.61518	0.35514	0.73175
2	C	-0.61516	-1.77264	-0.49138
2	C	-0.61516	-0.35600	-0.72316
2	C	0.61516	0.35763	-0.49087

Table 2: Unit cell of *up* structure. Layer division, atom types and positions for the *up* structure. The structure unit cell was divided in two layers corresponding to hydrogen and carbon atoms. tab:upunitcell

3.1 alt

sec:results-alt

In Fig. 3 we present the $\mathcal{V}^{x}$ spectra resulting from evaluate the Eq. (3) at using different polarization angles α in Eq. (1) for the C_16H_8-alt structure. The onset of the response is when the energy of the incoming light is the same of the gap energy. From this picture we can see that for the zone between the energy range of 0.90 eV-0.93 eV and polarization angles between 120° and 150° is the zone of the maximum response is held reaching values of $\mathcal{V}^{x}$ near to 30 Km/s. Also there is a second zone between the energy range of 0.70 eV-0.74 eV and same polarization angles where a local maximum of $\mathcal{V}^{x}$ reaching values near to 22 Km/s.We also found that the absolute maximum of the response is obtained for a polarization angle $\alpha = 145°$. The decomposition of $|\mathcal{V}^{a}|$ in the corresponding $\mathcal{V}^{x}$, $\mathcal{V}^{y}$, and $\mathcal{V}^{z}$ components is depicted in Fig. 4. From this figure we can see that for the energy range from 0.70 eV to 0.74 eV all the x, y, and z components contribute with almost the same intensity. In the other hand, for the energy range from 0.88 eV to 0.95 eV there is a major contribution coming from the $\mathcal{V}^{xz}$ component.

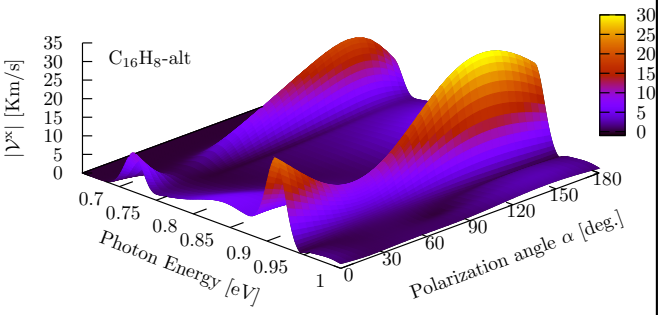

Figure 3: $\mathcal{V}^{x}$ for C_16H_8-alt structure. The maximum response zone is localized for an energy range from 0.90 eV to 0.93 eV. 145° and for a polarization angle of the incoming beam from 120° to 150°. fig:alt-magvxbincang

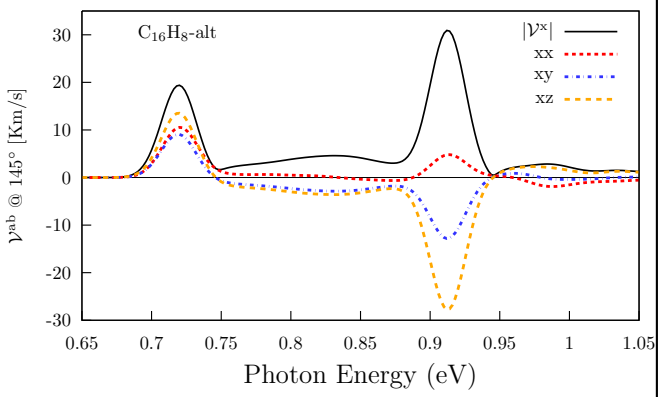

Figure 4: Three components of $\mathcal{V}^{x}$ @ 145°. fig:alt-vxb

3.1.1 $\mathcal{V}^y$

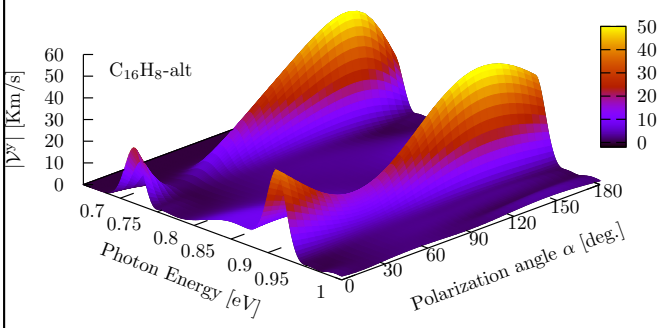

Figure 5: The most intense response for $\mathcal{V}^y$ is for 145°

fig:alt-magvybincang1

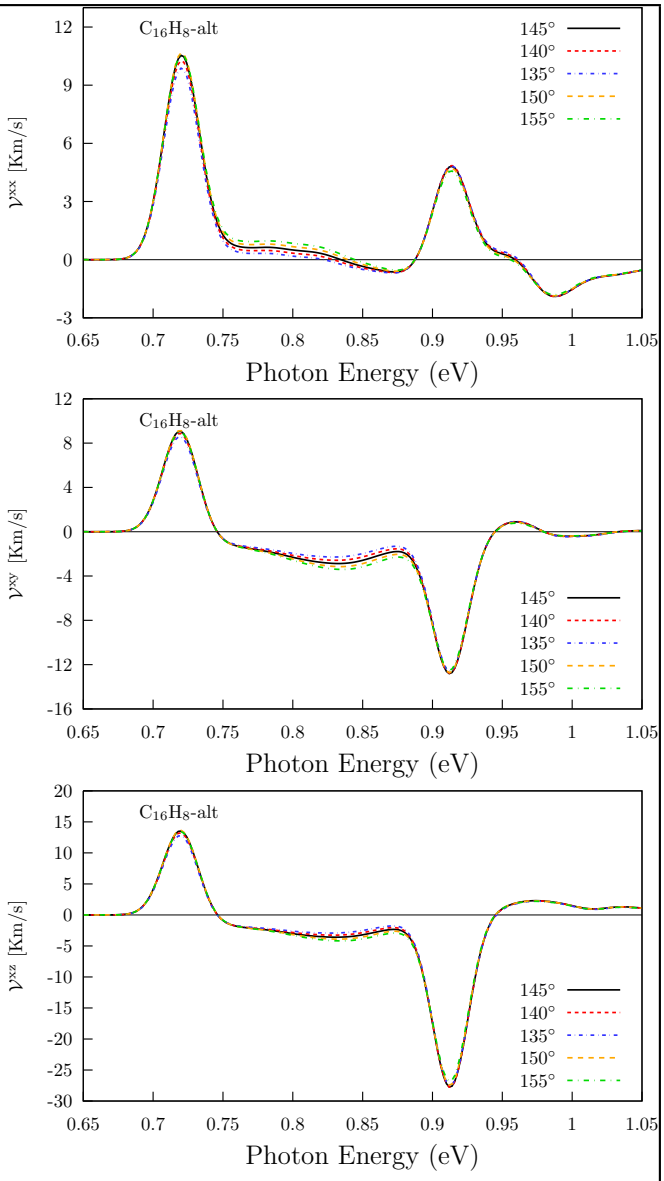

Figure 6: Cheking angle of incidence for yb components

fig:alt-ybangcomp

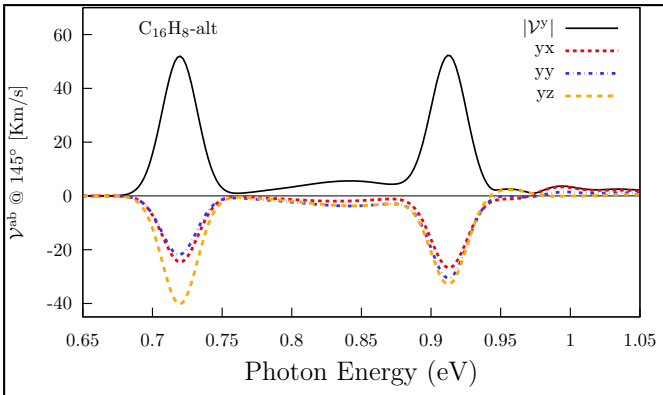

Figure 7: Three components of $\mathcal{V}^{y}$ @ 145°. fig:alt-vyb1

3.1.2 $|\mathcal{V}^{ab}|$, angles θ and φ, layers, and comparison with CdSe and GaAs.

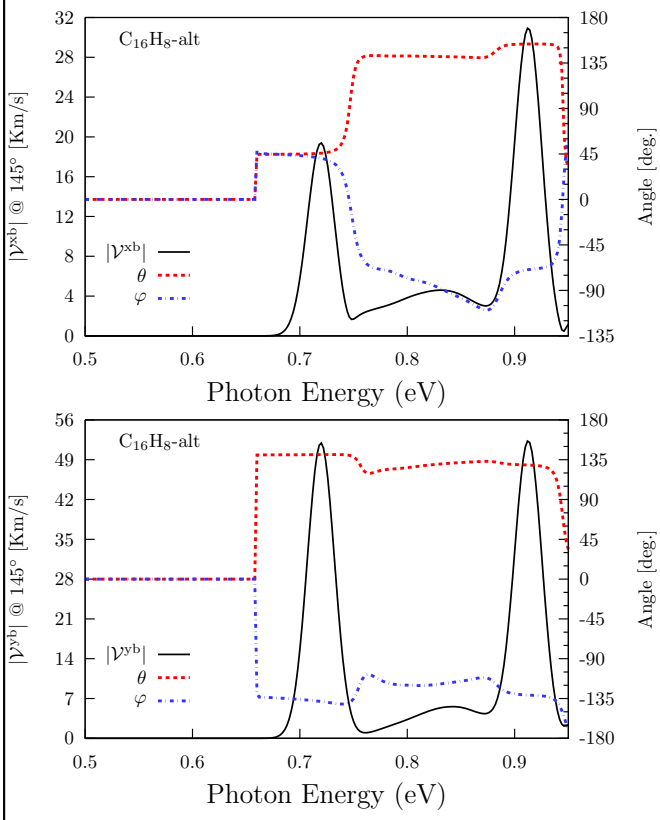

Figure 8: $|\mathcal{V}^{ab}|$ (solid line, leftside scale) and the corresponding angles θ and φ (dashed lines, rightside scale). fig:alt-rtp

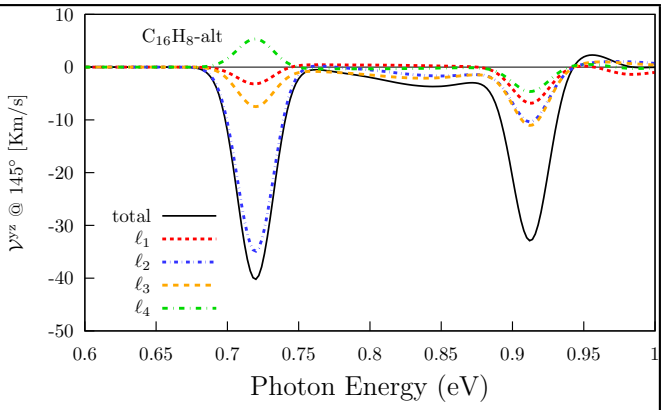

Figure 9: Layer decomposition for the most intense response: $\mathcal{V}^{yz}$. fig:alt-lay

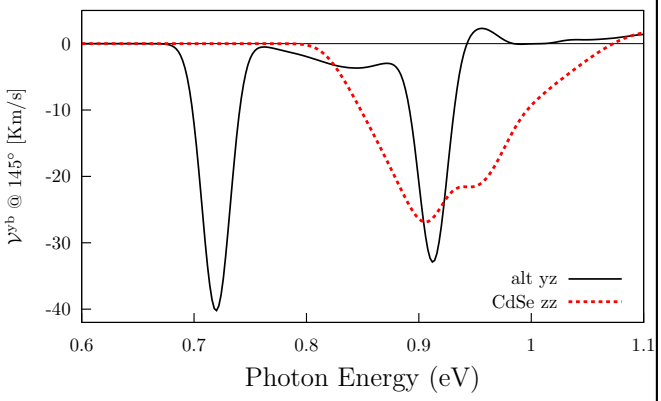

Figure 10: Comparisson of the most intense response vs the most intense responses of CdSe and GaAs. fig:alt-comp

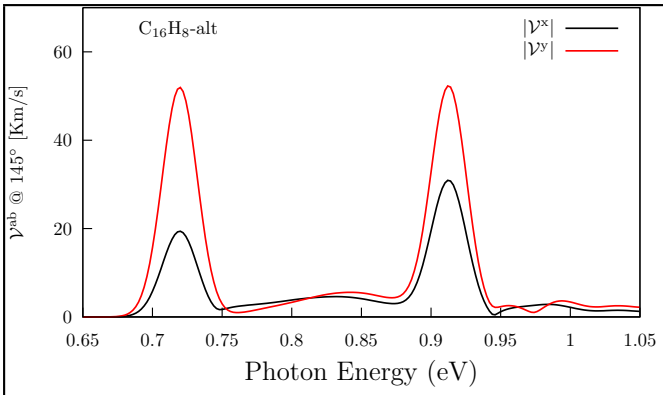

Figure 11: Comparisson of $|\mathcal{V}^{\mathrm{x}}|$ and $|\mathcal{V}^{\mathrm{y}}|$ fig:alt-xbybcomp

3.2 Up (graphone)

sec:results-up

3.2.1 $\mathcal{V}^{\mathrm{x}}$ energy range 0.0–0.2 eV

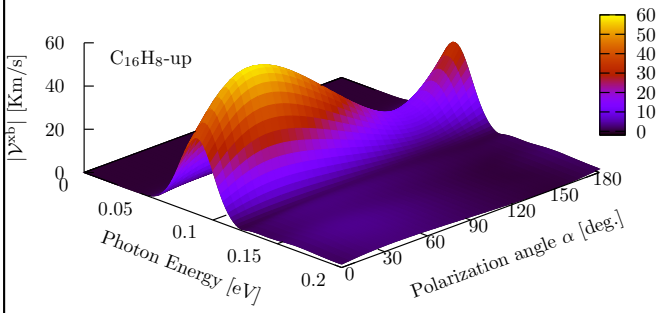

Figure 12: The most intense response for $\mathcal{V}^{\mathrm{x}}$ is for 40° fig:up-magvxbincang1

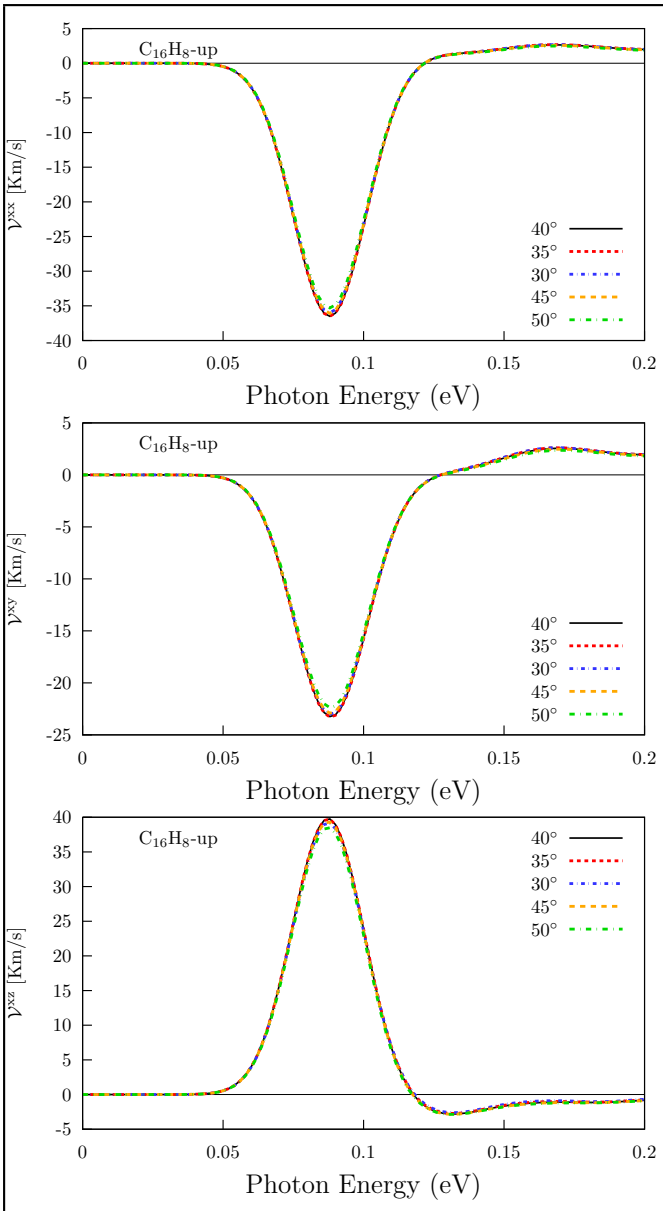

Figure 13: Cheking angle of incidence for xb components for up structure. `fig:up-xbangcomp`

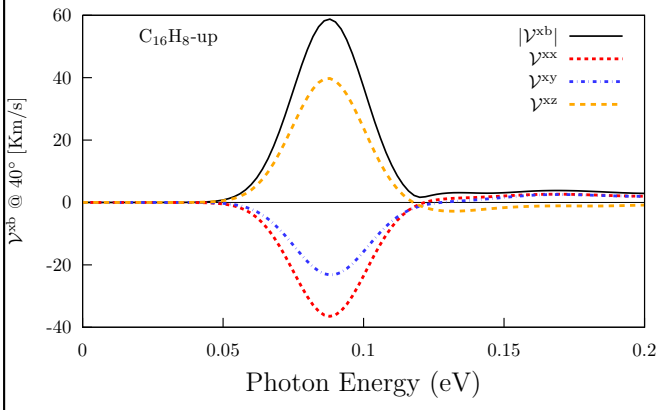

Figure 14: Three components of $\mathcal{V}^{x}$ @ 40° `fig:up-vxb1`

3.2.2 $\mathcal{V}^y$ energy range 0.0–0.2 eV

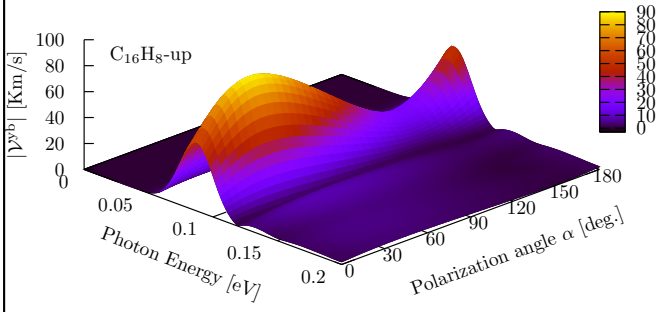

Figure 15: The most intense response for $\mathcal{V}^y$ is for 40°

fig:up-magvybincang1

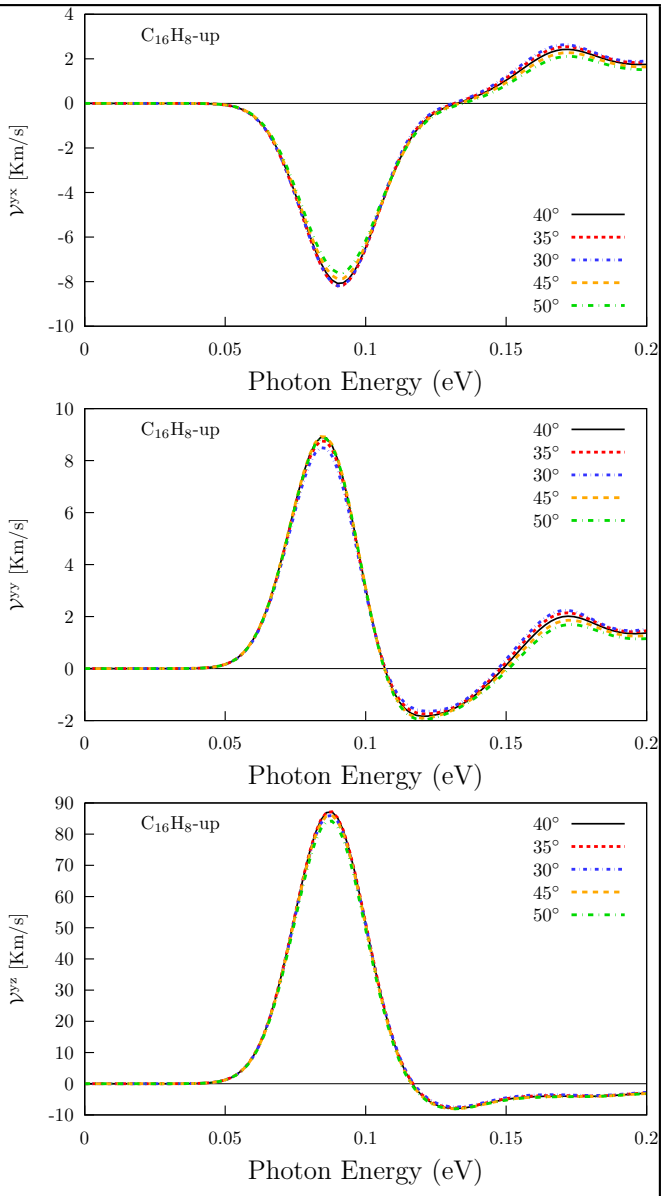

Figure 16: Cheking angle of incidence for *yb* components

fig:up-ybangcomp

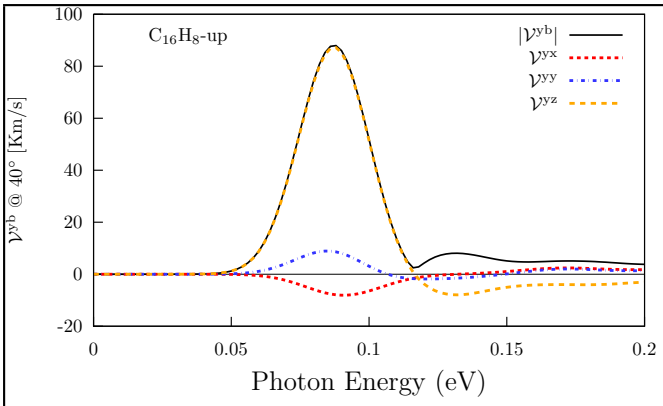

Figure 17: Three components of $\mathcal{V}^{y}$ @ 40°. fig:up-vyb1

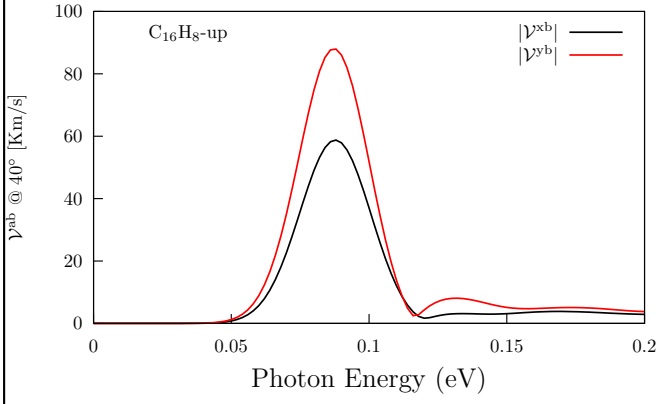

Figure 18: Comparisson of $|\mathcal{V}^{x}|$ and $|\mathcal{V}^{y}|$. fig:up-xbybcomp-1

3.2.3 $\mathcal{V}^{x}$ energy range 1.8–2.1 eV

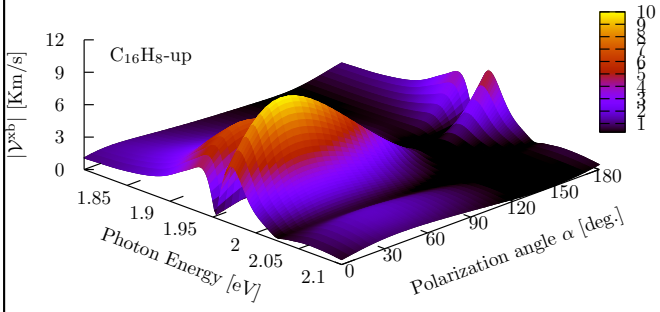

Figure 19: The most intense response for $\mathcal{V}^{x}$ is for 40°. fig:up-magxbincang2

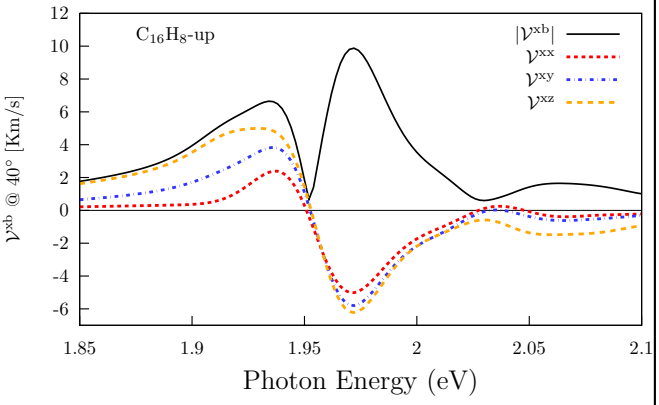

Figure 20: Three components of $\mathcal{V}^{x}$ @ 40°. fig:up-vxb2

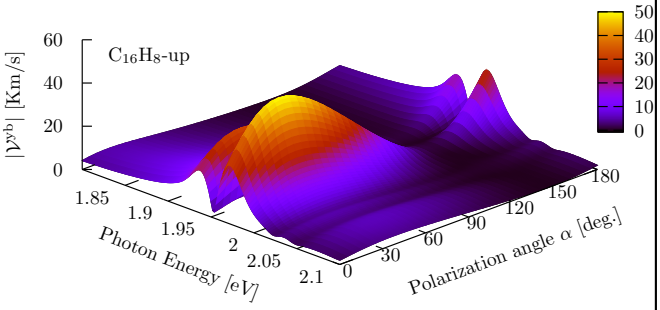

Figure 21: The most intense response for $\mathcal{V}^{y}$ is for 40°. fig:up-magybincang2

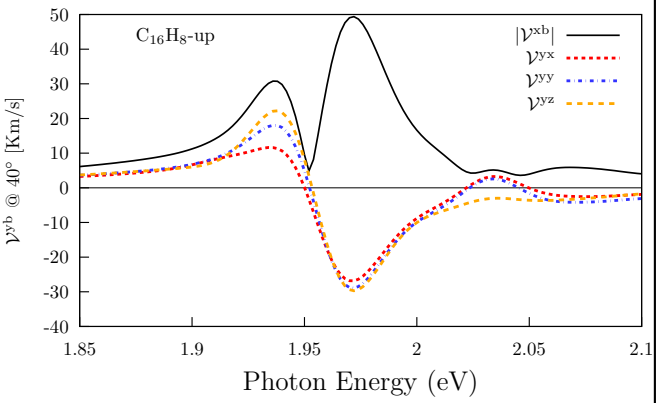

Figure 22: Three components of $\mathcal{V}^{y}$ @ 40°. fig:upvyb2

3.2.4 $|\mathcal{V}^{ab}|$, angles θ and φ, layers, and comparison with CdSe and GaAs for the energy range of 0.0–0.2 eV.

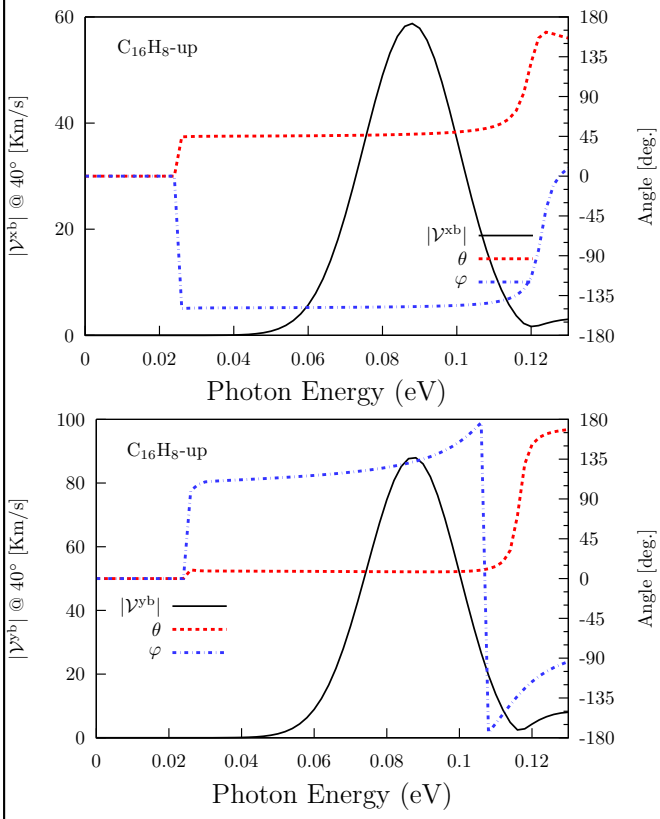

Figure 23: $|\mathcal{V}^{ab}|$ (solid line, leftside scale) and the corresponding angles θ and φ (dashed lines, rightside scale). fig:up-rtp1

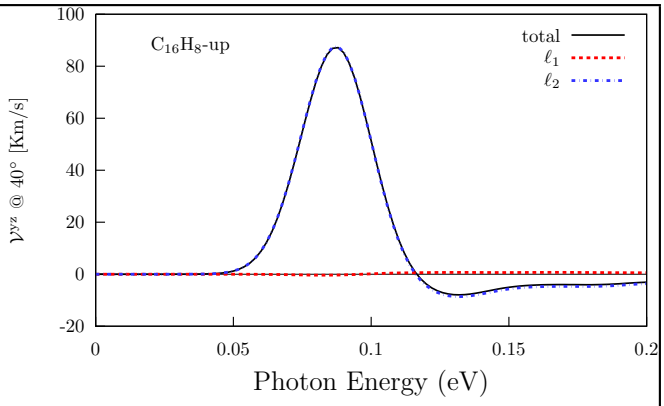

Figure 24: Layer decomposition for the most intense response: $\mathcal{V}^{yz}$. fig:up-lay1

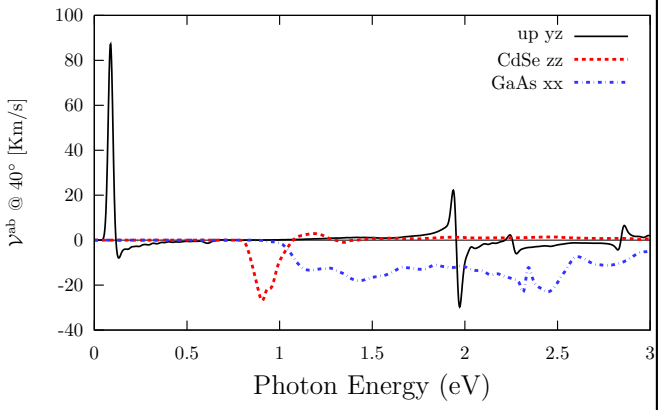

Figure 25: Comparisson of the most intense response vs the most intense responses of CdSe and GaAs. fig:up-comp1

3.2.5 $|\mathcal{V}^{ab}|$, angles θ and φ, layers, and comparison with CdSe and GaAs for the energy range of 1.8–2.1 eV

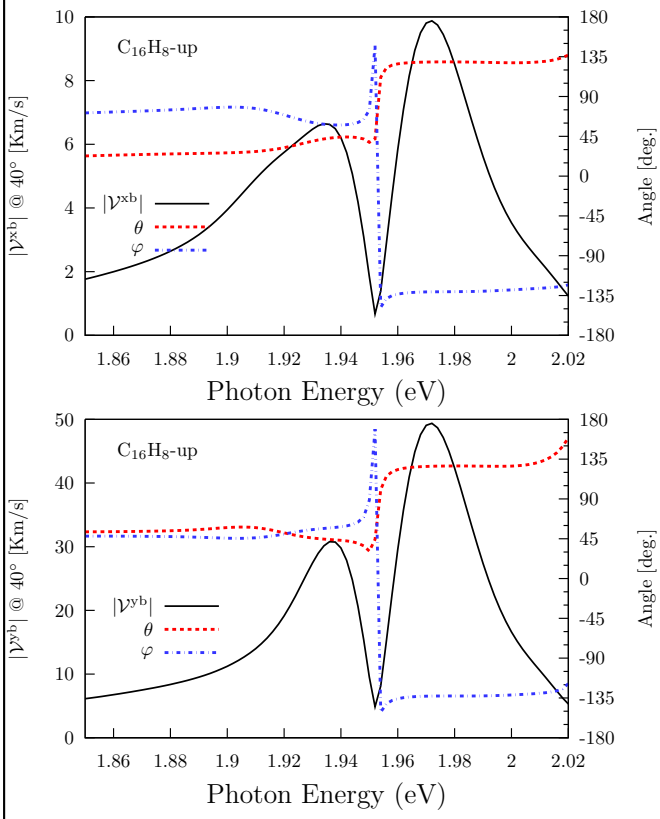

Figure 26: $|\mathcal{V}^{ab}|$ (solid line, leftside scale) and the corresponding angles θ and φ (dashed lines, rightside scale).

fig:up-rtp2

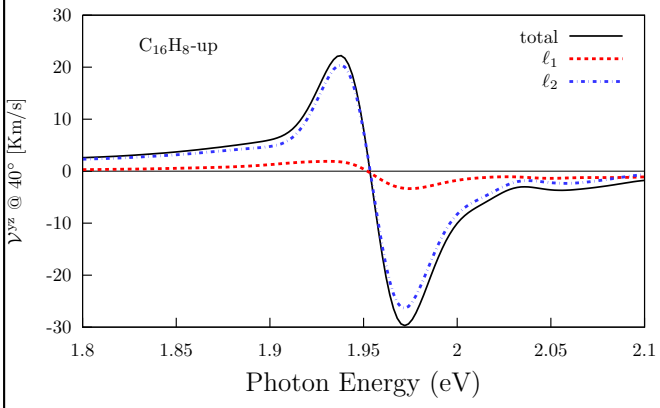

Figure 27: Layer decomposition for the most intense response: $\mathcal{V}^{yz}$.

fig:up-lay2

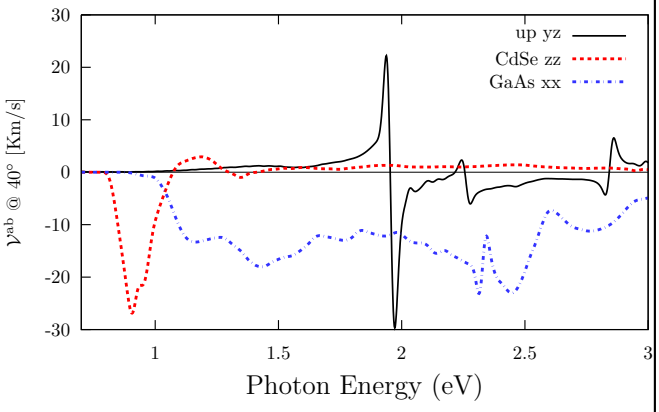

Figure 28: Comparisson of the most intense response vs the most intense responses of CdSe and GaAs.

fig:up-comp2

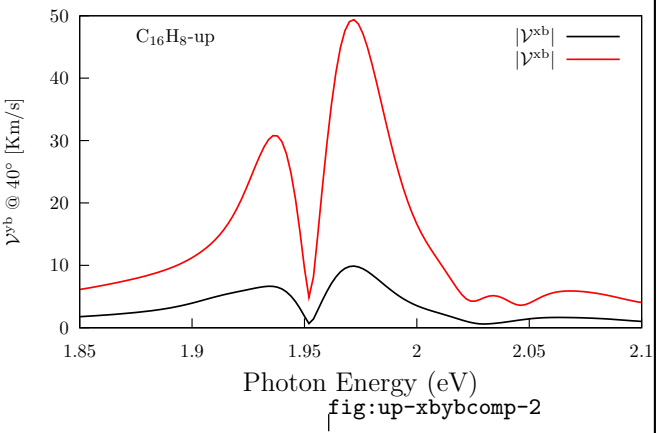

fig:up-xbybcomp-2

References

[1] X. Gonze, B. Amadon, P.-M. Anglade, J.-M. Beuken, F. Bottin, P. Boulanger, F. Bruneval, D. Caliste, R. Caracas, M. Côté, T. Deutsch, L. Genovese, Ph. Ghosez, M. Giantomassi, S. Goedecker, D.R. Hamann, P. Hermet, F. Jollet, G. Jomard, S. Leroux, M. Mancini, S. Mazevet, M.J.T. Oliveira, G. Onida, Y. Pouillon, T. Rangel, G.-M. Rignanese, D. Sangalli, R. Shaltaf, M. Torrent, M.J. Verstraete, G. Zerah, and J.W. Zwanziger. Abinit: First-principles approach to material and nanosystem properties. *Comput. Phys. Commun.*, 180(12):2582–2615, 2009.

[2] C. Hartwigsen, S. Goedecker, and J. Hutter. Relativistic separable dual-space gaussian pseudopotentials from h to rn. *Phys. Rev. B*, 58(7):3641, 1998.

[3] G. Onida, L. Reining, and A. Rubio. Electronic excitations: density-functional versus many-body greens-function approaches. *Rev. Mod. Phys.*, 74(2):601, 2002.

[4] Reinaldo Zapata-Peña, Sean M Anderson, Bernardo S Mendoza, and Anatoli I Shkrebtii. Nonlinear optical responses in hydrogenated graphene structures. *physica status solidi (b)*, 253(2):226–233, 2016.